

**Topology optimization subject to additive
manufacturing constraints**

Moritz Ebeling-Rump¹, Dietmar Hömberg¹, Robert Lasarzik¹, Thomas Petzold²

submitted: October 9, 2019

¹ Weierstrass Institute
Mohrenstr. 39
10117 Berlin
Germany
E-Mail: moritz.ebeling-rump@wias-berlin.de
dietmar.hoemberg@wias-berlin.de
robert.lasarzik@wias-berlin.de

² inpro
Innovationsgesellschaft für fortgeschrittene
Produktionssysteme in der Fahrzeugindustrie mbH
Steinplatz 2
10623 Berlin
Germany
E-Mail: Thomas.Petzold@inpro.de

No. 2629
Berlin 2019



2010 *Mathematics Subject Classification.* 49Q10, 74P05, 49Q20, 65M60, 74P10.

Key words and phrases. Additive manufacturing, topology optimization, linear elasticity, phase field method, optimality conditions, numerical simulations.

Edited by
Weierstraß-Institut für Angewandte Analysis und Stochastik (WIAS)
Leibniz-Institut im Forschungsverbund Berlin e. V.
Mohrenstraße 39
10117 Berlin
Germany

Fax: +49 30 20372-303
E-Mail: preprint@wias-berlin.de
World Wide Web: <http://www.wias-berlin.de/>

Topology optimization subject to additive manufacturing constraints

Moritz Ebeling-Rump, Dietmar Hömberg, Robert Lasarzik, Thomas Petzold

Abstract

In Topology Optimization the goal is to find the ideal material distribution in a domain subject to external forces. The structure is optimal if it has the highest possible stiffness. A volume constraint ensures filigree structures, which are regulated via a Ginzburg-Landau term. During 3D Printing overhangs lead to instabilities, which have only been tackled unsatisfactorily. The novel idea is to incorporate an Additive Manufacturing Constraint into the phase field method. A rigorous analysis proves the existence of a solution and leads to first order necessary optimality conditions. With an Allen-Cahn interface propagation the optimization problem is solved iteratively. At a low computational cost the Additive Manufacturing Constraint brings about support structures, which can be fine tuned according to engineering demands. Stability during 3D Printing is assured, which solves a common Additive Manufacturing problem.

1 Introduction

Additive Manufacturing or *3D Printing* is understood as the process of building up a structure layer by layer. Traditional manufacturing methods, such as *Injection Molding*, place constraints on the achievable shapes. Whereas with 3D Printing the complexity of the possible forms is much less limited. Traditional methods allow for a cheaper and faster production in high volume orders. However, as order volumes decrease and need for customizability increases, Additive Manufacturing becomes more attractive. It allows for production of parts just in time as they are needed. This reduces the logistical burden tremendously. Some even call 3D Printing the next industrial revolution and draw comparisons to feats such as the assembly line.

Additive Manufacturing comes with its own constraints and problems. The production of a single unit takes longer and the surface structure has a rougher finish.

This paper focuses on eliminating instabilities during the printing process which are caused by overhangs. These are problematic in *Fused Deposition Modeling*, where a plastic filament is heated and extruded. Printing layer by layer can leave overhangs disconnected from the rest of the structure or cause sagging filament. Commonly external support structures are added to alleviate that problem. On the downside, this method uses more material and takes longer to print. Removing support structures after the printing process is both time and labor intensive.

The problem of instabilities can be alleviated by incorporating an Additive Manufacturing Constraint (AMC) in the modeling stage. Rigidity of the structure during the building process is taken into consideration. When executing the Topology Optimization, the AMC is accounted for via a penalty term. While being printed the resulting structure shall be stable without relying on manually added supports. This approach is introduced in the work of (Allaire *et al.*, 2017a) and results are presented in (Allaire *et al.*, 2017b).

As a novel approach the AMC is incorporated into the phase field method for Topology Optimization. An analysis of the optimal control problem subject to Additive Manufacturing Constraints shows existence of a solution and leads to optimality conditions. The proofs are adapted from the scheme developed by (Blank *et al.*, 2014). This approach is validated numerically by showing that the AMC increases stability during the manufacturing process.

This paper is partitioned in the following way: After explaining linear elasticity the theoretical foundation of topology optimization is laid out in Section 2.3. The Additive Manufacturing Constraint is introduced in Section 2.4 and incorporated into the optimal control problem. Existence of a unique solution and a rigorous derivation of optimality conditions is displayed in Passage 3. Numerical approaches are explained in Chapter 4. To examine the influence of the Additive Manufacturing Constraint, calculations are done with and without it in Chapter 5.

2 Problem Formulation

The aim of this section is to define the optimal control problem. After modeling the mechanics, topology optimization is explained and the Additive Manufacturing Constraint is formalized. First of all some notations are introduced.

2.1 Notation

Let $\Omega \subset \mathbb{R}^d$, $d = 2, 3$ be a bounded, regular domain and denote its boundary by Γ . In case of a Dirichlet boundary $\Gamma_D \subset \partial\Omega$ the notation

$$H_D^1(\Omega, \mathbb{R}^d) := \{\xi \in H^1(\Omega, \mathbb{R}^d) \mid \xi = 0 \text{ on } \Gamma_D\}$$

is used.

The Frobenius inner product for second order tensors \mathcal{M}, \mathcal{N} is defined by the pairwise sum of element-products

$$\mathcal{M} : \mathcal{N} := \sum_{i,j=1}^d \mathcal{M}_{ij} \mathcal{N}_{ij}.$$

The bilinear form is displayed using

$$\langle \mathcal{M}, \mathcal{N} \rangle_C := \int_{\Omega} C \mathcal{M} : \mathcal{N} \, dx. \quad (1)$$

Note that $C \mathcal{M}$ is defined via

$$[C \mathcal{M}]_{ij} := \sum_{k=1}^d \sum_{l=1}^d C_{ijkl} \mathcal{M}_{kl},$$

where C is a fourth order tensor.

2.2 Linear Elasticity Problem

Using the *displacement* $u : \Omega \rightarrow \mathbb{R}^d$ the *linearized strain tensor*

$$\mathcal{E}(u) := \frac{1}{2} (\nabla u + \nabla u^T) \quad (2)$$

is defined.

The material distribution $\varphi \in L^\infty(\Omega)$ will be introduced in section (2.3). Consider the symmetric fourth order stiffness tensor $C(\varphi)$ with continuously differentiable entries. It is assumed that the derivative of the stiffness tensor $C'(\varphi)$ is globally Lipschitz continuous. Towards receiving pure phases, a transition function $s(\varphi) = \varphi^3$ is employed. The elasticity tensor for the whole domain is defined in the following way

$$C(\varphi) := C_{mat}s(\varphi) + C_{void}(1 - s(\varphi)), \quad (3)$$

where

$$\begin{aligned} C_{mat}\mathcal{E} &:= \lambda_{mat}\text{tr}(\mathcal{E})I + 2\mu_{mat}\mathcal{E}, \\ C_{void}\mathcal{E} &:= \epsilon^2 C_{mat}\mathcal{E}. \end{aligned} \quad (4)$$

The constants λ_{mat} and μ_{mat} are called Lamé parameters. This definition warrants $0 \neq C_{void} \ll C_{mat}$, which ensures low stiffness in void, but avoids degeneracy.

A load f is acting on a part of the boundary labeled Γ_f and gravitational force g is present where material φ is located. Let $u^m \in H_D^1(\Omega, \mathbb{R}^d)$ be the unique weak solution of the mechanical linear elasticity problem (P^m) . This means that u^m satisfies the weak formulation of the mechanical system for all $v^m \in H_D^1(\Omega, \mathbb{R}^d)$, see Equation (6). Such a function u^m exists, as proven in Theorem 3.1. The superscript m is used throughout this paper in connection with the mechanical system. The normal vector is denoted by n .

Mechanical system

$$(P^m) \begin{cases} -\text{div}[C(\varphi)\mathcal{E}(u^m)] = \varphi g & \text{in } \Omega \\ u^m = 0 & \text{on } \Gamma_D \\ [C(\varphi)\mathcal{E}(u^m)]n = 0 & \text{on } \partial\Omega \setminus (\bar{\Gamma}_D \cup \bar{\Gamma}_f) \\ [C(\varphi)\mathcal{E}(u^m)]n = f & \text{on } \Gamma_f, \end{cases} \quad (5)$$

Weak formulation

$$\langle \mathcal{E}(u^m), \mathcal{E}(v^m) \rangle_{C(\varphi)} = F(v^m, \varphi) \quad \forall v^m \in H_D^1(\Omega, \mathbb{R}^d), \quad (6)$$

$$\text{where } F(v^m, \varphi) := \int_{\Omega} \varphi g \cdot v^m \, dx + \int_{\Gamma_f} f \cdot v^m \, d\omega.$$

2.3 Topology Optimization

This section is based on (Blank *et al.*, 2013). Topology Optimization is concerned with the optimal distribution of a limited quantity of material in a domain Ω . The distribution of material in Ω is described by a *phase field* φ with

$$0 \leq \varphi \leq 1 \quad (7)$$

almost everywhere in Ω . Here $\varphi = 0$ describes void and $\varphi = 1$ represents areas containing material. In a physically accurate setting each point in space either does or does not contain material, i.e. $\varphi \in \{0, 1\}$, leading to a *sharp transition*. However, in the realm of optimization a *smooth transition* between material and void is desired in order to calculate derivatives. This is achieved by explicitly

allowing *impure phases*, i.e. states with $0 < \varphi < 1$. The transition is seen as the interface between material and void.

Without further restrictions the solution would be trivial. The stiffest structure is produced by setting $\varphi \equiv 1$ on Ω , i.e. covering the whole domain with material. An additional constraint makes the problem more interesting. Let m be the *mass parameter* with $0 < m < 1$. The amount of material is restricted via a *volume constraint*

$$\int_{\Omega} \varphi \, dx = m|\Omega|, \quad (8)$$

where $|\Omega|$ denotes the Lebesgue measure of the domain Ω . The admissible set is defined as

$$\mathcal{G}^m := \left\{ \varphi \in H^1(\Omega, \mathbb{R}) \mid 0 \leq \varphi(x) \leq 1 \text{ a.e. in } \Omega \text{ and } \int_{\Omega} \varphi \, dx = m|\Omega| \right\}.$$

The objective is to find a material distribution $\varphi \in \mathcal{G}^m$ and a corresponding solution of the elasticity problem $u : \Omega \rightarrow \mathbb{R}^d$ such that the *mean compliance*

$$F(u, \varphi) \quad (9)$$

is minimized. However, this minimization problem is not well-posed as explained in (Allaire *et al.*, 2004). The regularity of the solution is not ensured. In computational examples this can lead to a checkerboard solution. *Checkerboarding* is the frequent occurrence of jumps between material and void, which is not desirable, see (Shukla *et al.*, 2013). The algorithm might produce so called *porous* solutions, which can be thought of as sponge-like microstructures. In many industrial cases this type of material is hard to realize and therefore undesirable. The ill-posedness can be alleviated by adding a *perimeter regularization* which was proven in (Ambrosio & Buttazzo, 1993). The paper of (Takezawa *et al.*, 2010) explains that the perimeter can be approximated by the *Ginzburg-Landau term*

$$E^\epsilon(\varphi) := \int_{\Omega} \frac{\epsilon}{2} |\nabla \varphi|^2 + \frac{1}{\epsilon} \psi(\varphi) \, dx, \quad (10)$$

for $\epsilon > 0$ and $\varphi \in H^1(\Omega, \mathbb{R})$. This function finds its origin in the work of (Ginzburg & Landau, 1950). For convergence properties as ϵ approaches zero see (Van Gennip *et al.*, 2012). The first term penalizes transitions between material and void through the gradient of the material distribution. A commonly used potential $\psi(\varphi)$ is the *double well potential*

$$\psi(\varphi) = \frac{1}{4} ((\varphi - 1)\varphi)^2 = \frac{1}{4} (\varphi^2 - \varphi)^2.$$

The aim of the potential is to penalize impure phases, which are states where the phase field φ is not equal to 0 or 1.

Assumption A1. There exist positive constants $\underline{\Lambda}$, $\bar{\Lambda}$ and Λ' such that for all symmetrical $\mathcal{M}, \mathcal{N} \in \mathbb{R}^{d \times d} \setminus \{0\}$ and all $\varphi, \omega \in \mathbb{R}$ the following relationships hold:

$$\underline{\Lambda} |\mathcal{M}|^2 \leq C(\varphi) \mathcal{M} : \mathcal{M} \leq \bar{\Lambda} |\mathcal{M}|^2, \quad (11)$$

$$|C'(\varphi) \omega \mathcal{M} : \mathcal{N}| \leq \Lambda' |\omega| |\mathcal{M}| |\mathcal{N}|. \quad (12)$$

Assumption A2. The data lays in L^2

$$f \in L^2(\Gamma_f, \mathbb{R}^d), \quad g \in L^2(\Omega, \mathbb{R}^d).$$

2.4 Additive Manufacturing Constraint

In Additive Manufacturing a structure is created in a layer-by-layer approach. Following (Allaire *et al.*, 2017a) the intermediate states are taken into consideration to ensure stability during manufacturing. This can be thought of as slicing the final topology into horizontal layers and leads to the definition of the *intermediate shape* up to height $h \in \mathbb{R}_+$

$$\Omega_h := \Omega \cap \{x = (x_1, \dots, x_d) \in \mathbb{R}^d, 0 \leq x_d \leq h\}.$$

Whenever $\langle \cdot, \cdot \rangle$ contains terms with index h the integration takes place over the intermediate domain Ω_h , instead of Ω .

The Dirichlet boundary for the AMC problems differs from the Dirichlet boundary of the mechanical problem. In the mechanical problem it describes areas where the structure is supported when forces are applied. In the constraint problems the process of Additive Manufacturing is simulated. Homogeneous Dirichlet boundary conditions are assumed for all parts of the geometry touching the building plate Γ_0 . During the manufacturing process no surface forces are applied to the structure. Each intermediate shape Ω_h is only subjected to gravity g .

The elastic displacement $u_h^c \in H_D^1(\Omega_h, \mathbb{R}^d)$ is defined as the unique weak solution of the problem (P_h^c) . Each function u_h^c satisfies the weak formulation of the AMC systems, i.e. Equation (14), on the corresponding space Ω_h .

AMC system

$$(P_h^c) \begin{cases} -\operatorname{div} [C(\varphi) \mathcal{E}(u_h^c)] = \varphi g & \text{in } \Omega_h \\ u_h^c = 0 & \text{on } \Gamma_0 \\ [C(\varphi) \mathcal{E}(u_h^c)] n = 0 & \text{on } \partial\Omega \setminus \bar{\Gamma}_0, \end{cases} \quad (13)$$

Weak formulation

$$\langle \mathcal{E}(u_h^c), \mathcal{E}(v_h) \rangle_{C(\varphi)} = \int_{\Omega_h} \varphi g \cdot v_h \, dx \quad \forall v_h \in H_D^1(\Omega_h, \mathbb{R}^d). \quad (14)$$

The mechanical system (5) described the load case where a force is acting on the structure. On the other hand the AMC system (13) models the printing process, where only gravity is considered. To help distinguish between both systems the superscript c is used in conjunction with constraint problems.

In order to judge the stiffness during the manufacturing process, the compliance of the intermediate shape Ω_h

$$c_{\Omega_h} := \int_{\Omega_h} \varphi g \cdot u_h^c \, dx$$

is defined. Low compliance values are desirable, because they coincide with high stiffness. A penalty function is defined via

$$P(u^c, \varphi) := \int_0^H \int_{\Omega_h} \varphi g \cdot u_h^c \, dx \, dh.$$

The idea is to slice the domain Ω into N layers and define successively growing domains Ω_h with $\Omega_i \subseteq \Omega_j$ for $i \leq j$. Up to this point the height h has been a continuous parameter. To avoid double subscripts it is now used as an index of the domain. For example, u_h^c is the displacement of the structure up to the h -th layer. The following notation is used:

$$u^c := \{u_h^c\}_{h=1}^N \in H_D^1(\Omega_1, \mathbb{R}^d) \times \dots \times H_D^1(\Omega_N, \mathbb{R}^d) =: H^c.$$

The outer integration of $P(u^c, \varphi)$ becomes a sum yielding the discretized penalty function

$$P^d(u^c, \varphi) := \sum_{h=1}^N \int_{\Omega_h} \varphi g \cdot u_h^c \, dx.$$

Not only the final structure shall bend as little as possible, but also all intermediate structures. Towards calculating the penalty function an additional N stationary problems have to be solved.

All ingredients have been gathered to write down the optimization problem.

$$(P^\epsilon) \begin{cases} \min & J^\epsilon(u^m, u^c, \varphi) := F(u^m, \varphi) + \beta P^d(u^c, \varphi) + \gamma E^\epsilon(\varphi) \\ \text{over} & (u^m, u^c, \varphi) \in H_D^1(\Omega, \mathbb{R}^d) \times H^c \times H^1(\Omega, \mathbb{R}) \\ \text{s.t.} & (u^m, \varphi) \text{ fulfills (6) on } \Omega, \\ & (u_h^c, \varphi) \text{ fulfills (14) on } \Omega_h, \, h = 1, \dots, N \\ & \text{and } \varphi \in \mathcal{G}^m. \end{cases}$$

3 Analysis of the Optimal Control Problem

The aim of this chapter is to prove optimality conditions. Theorems and proofs of this chapter are adapted from the work of (Blank *et al.*, 2014).

Theorem 3.1. For a given phase field $\varphi \in L^\infty(\Omega)$ there exists a unique weak solution $u \in H_D^1(\Omega, \mathbb{R}^d)$ of the elasticity problem (P^m) such that the weak formulation of the elasticity problem (6) is fulfilled. There exists a constant $c = c(f, g) > 0$ such that

$$\|u\|_{H_D^1(\Omega, \mathbb{R}^d)} \leq c (\|\varphi\|_{L^\infty(\Omega)} + 1). \quad (15)$$

The proof is a standard application of Lax-Milgram. It utilizes Korn's inequality, Hölder's inequality, Poincaré-Friedrichs inequality and the trace theorem.

Theorem 3.1 defines the *control-to-state operator* which maps the phase field φ to the unique weak solution u of the elasticity problem

$$S : L^\infty(\Omega) \rightarrow H_D^1(\Omega, \mathbb{R}^d), \quad S(\varphi) := u.$$

In order to derive first-order necessary optimality conditions the states will be replaced by the control-to-state operators. This results in a reduced functional which only depends on the control φ . When the reduced functional is differentiated, the differentiability of the control-to-state operator comes into play via the chain rule. Towards the Fréchet-differentiability of the operator S , the following Lipschitz continuity is needed.

Lemma 3.2. Let there be controls $\varphi_i \in L^\infty(\Omega, \mathbb{R})$ and corresponding states $u_i = S(\varphi_i)$, $i = 1, 2$. Then there exists a constant $c > 0$ such that

$$\|u_1 - u_2\|_{H_D^1(\Omega, \mathbb{R}^d)} \leq c \|\varphi_1 - \varphi_2\|_{L^\infty(\Omega, \mathbb{R})}. \quad (16)$$

The proof is done by subtracting the corresponding elasticity equations from one another and applying the triangle inequality, Lipschitz continuity of $C(\varphi)$, Korn's and Hölder's inequality and Poincaré-Friedrich. Details can be found in (Blank *et al.*, 2014).

Theorem 3.3. The control-to-state operator S is Fréchet-differentiable. The derivative at $\varphi \in L^\infty(\Omega, \mathbb{R})$ in direction $\omega \in L^\infty(\Omega, \mathbb{R})$ is

$$S'(\varphi)\omega = \bar{u}, \quad (17)$$

with $u = S(\varphi)$ and \bar{u} being the unique solution of

$$\langle \mathcal{E}(\bar{u}), \mathcal{E}(v) \rangle_{C(\varphi)} = -\langle \mathcal{E}(u), \mathcal{E}(v) \rangle_{C'(\varphi)\omega} + \int_{\Omega} \omega g \cdot v \, dx \quad (18)$$

for all $v \in H_D^1(\Omega, \mathbb{R}^d)$. Furthermore there exists a constant $c > 0$ such that

$$\|\bar{u}\|_{H_D^1(\Omega, \mathbb{R}^d)} \leq c \|\omega\|_{L^\infty(\Omega, \mathbb{R})}. \quad (19)$$

Thus $S'(\varphi)$ is a bounded operator.

Remark. Formally this can be seen by differentiating the implicit state equation

$$\langle \mathcal{E}(S(\varphi)), \mathcal{E}(v) \rangle_{C(\varphi)} = F(v, \varphi)$$

with respect to φ in direction ω .

The proof applies Assumption (A1), Theorem 3.1 and Lemma 3.2. Additionally standard tools like Korn's and Hölder's inequality are used. For a complete proof see (Blank *et al.*, 2014).

Notice that these results carry over to the differentiability of the control-to-state operator S^m of the mechanical system as well as the control-to-state operators S_h^c , $h = 1, \dots, N$ of the AMC problems. The following notation will be used:

$$\begin{aligned} S^m : L^\infty(\Omega) &\rightarrow H_D^1(\Omega, \mathbb{R}^d), \quad S^m(\varphi) := u^m \\ S_h^c : L^\infty(\Omega) &\rightarrow H_D^1(\Omega_h, \mathbb{R}^d), \quad S_h^c(\varphi) := u_h^c, \quad h = 1, \dots, N, \\ S^c : L^\infty(\Omega) &\rightarrow H^c, \quad S^c(\varphi) := u^c. \end{aligned}$$

The space $L^\infty(\Omega)$ has to be restricted to $L^\infty(\Omega_h)$ if S_h^c is applied.

Theorem 3.4. Under assumptions (A1) and (A2) there exists a solution to the optimization problem (P^ϵ) .

Proof. The existence of a unique solution to the elasticity problem (6) is ensured by Theorem 3.1. Let the *admissible set* be defined by

$$\begin{aligned} F_{ad} := \{ & (u^m, u^c, \varphi) \in H_D^1(\Omega, \mathbb{R}^d) \times H^c \times \mathcal{G}^m, \\ \text{s.t.} & (u^m, \varphi) \text{ fulfills (6) on } \Omega, \\ & (u_h^c, \varphi) \text{ fulfills (14) on } \Omega_h, \quad h = 1, \dots, N \}. \end{aligned}$$

Looking at (6) with $v^m := u^m$ for (P^m) and at (14) with $v_h := u_h^c$ for (P_h^c) , $h = 1, \dots, N$ it can be seen that J^ϵ has a lower bound on the non-empty set F_{ad} since

$$\begin{aligned} J^\epsilon(u^m, u^c, \varphi) &= F(u^m, \varphi) + \beta P^d(u^c, \varphi) + \gamma E^\epsilon(\varphi) \\ &= \int_{\Omega} C(\varphi) \mathcal{E}(u^m) : \mathcal{E}(u^m) \, dx + \beta \sum_{h=1}^N \int_{\Omega_h} C(\varphi) \mathcal{E}(u_h^c) : \mathcal{E}(u_h^c) \, dx \\ &\quad + \gamma \int_{\Omega} \frac{\epsilon}{2} |\nabla \varphi|^2 + \frac{1}{\epsilon} \psi(\varphi) \, dx \\ &\stackrel{(11)}{\geq} \int_{\Omega} \underline{\Lambda} |\mathcal{E}(u^m)|^2 \, dx + \beta \sum_{h=1}^N \int_{\Omega_h} \underline{\Lambda} |\mathcal{E}(u_h^c)|^2 \, dx + \gamma \int_{\Omega} \frac{\epsilon}{2} |\nabla \varphi|^2 + \frac{1}{\epsilon} \psi(\varphi) \, dx \\ &\geq 0. \end{aligned}$$

Thus

$$\inf_{(u^m, u^c, \varphi) \in F_{ad}} J^\epsilon(u^m, u^c, \varphi) > -\infty$$

holds. Let

$$\{(u_k^m, u_k^c, \varphi_k)\} \subset F_{ad}, \quad k \in \mathbb{N}$$

be a minimizing sequence with

$$\lim_{k \rightarrow \infty} J^\epsilon(u_k^m, u_k^c, \varphi_k) = \inf_{(u^m, u^c, \varphi) \in F_{ad}} J^\epsilon(u^m, u^c, \varphi).$$

First note that $\{\varphi_k\} \subset \mathcal{G}^m$ is uniformly bounded. Applying the estimation (15), it is clear that the sequences $\{u_k^m\}$ and $\{u_{h,k}^c\}$, $h = 1, \dots, N$ are bounded independently of k in $H_D^1(\Omega, \mathbb{R}^d)$ and $H_D^1(\Omega_h, \mathbb{R}^d)$, $h = 1, \dots, N$ respectively. For every bounded sequence there exists a weakly convergent subsequence

$$\begin{aligned} u_k^m &\rightharpoonup \overline{u^m} && \text{in } H_D^1(\Omega, \mathbb{R}^d) \\ u_{h,k}^c &\rightharpoonup \overline{u_h^c} && \text{in } H_D^1(\Omega_h, \mathbb{R}^d), \quad h = 1, \dots, N \\ \varphi_k &\rightharpoonup \overline{\varphi} && \text{in } H^1(\Omega, \mathbb{R}). \end{aligned} \quad (20)$$

The set \mathcal{G}^m is convex and closed in $H_D^1(\Omega, \mathbb{R})$ hence weakly closed, thus $\overline{\varphi} \in \mathcal{G}^m$. Moreover the above convergences hold strongly in L^2 . Choosing another subsequence denoted in the same way leads to pointwise convergence

$$\varphi_k \longrightarrow \overline{\varphi} \quad \text{a.e. in } \Omega. \quad (21)$$

The functionals F and P^d are continuous with respect to the underlying topologies. Using the convergence results from above and noting that the norm is weakly lower semi-continuous and the potential is continuous, thus weakly lower semi-continuous, the following inequality is obtained

$$J^\epsilon(\overline{u^m}, \overline{u^c}, \overline{\varphi}) \leq \liminf_{k \rightarrow \infty} J^\epsilon(u_k^m, u_k^c, \varphi_k).$$

It is left to show that the elasticity problem is fulfilled by $(\overline{u^m}, \overline{\varphi})$ on Ω and $(\overline{u_h^c}, \overline{\varphi})$ on Ω_h , $h = 1, \dots, N$, respectively. For the mechanical problem as well as the constraint problems the bilinear form of the elasticity problem has to be passed to the limit. Only the mechanical case will be considered since the other cases are analogous. The sequence $\{\varphi_k\}$ is uniformly bounded since $\{\varphi_k\} \subset \mathcal{G}^m$. Using pointwise convergence (21) Lebesgue's dominated convergence theorem can be employed to get strong convergence of $C(\varphi_k) \mathcal{E}(v)$ to $C(\overline{\varphi}) \mathcal{E}(v)$ in $L^2(\Omega, \mathbb{R}^{d \times d})$. Taking into account the weak convergence properties from above this yields

$$\int_{\Omega} C(\varphi_k) \mathcal{E}(u_k^m) : \mathcal{E}(v) \, dx \longrightarrow \int_{\Omega} C(\overline{\varphi}) \mathcal{E}(\overline{u^m}) : \mathcal{E}(v) \, dx \quad (22)$$

for all $v \in H_D^1(\Omega, \mathbb{R}^d)$. Finally the calculation arrives at

$$\begin{aligned} -\infty < \inf_{(u^m, u^c, \varphi) \in F_{ad}} J^\epsilon(u^m, u^c, \varphi) &\leq J^\epsilon(\overline{u^m}, \overline{u^c}, \overline{\varphi}) \\ &\leq \liminf_{k \rightarrow \infty} J^\epsilon(u_k^m, u_k^c, \varphi_k) \\ &= \inf_{(u^m, u^c, \varphi) \in F_{ad}} J^\epsilon(u^m, u^c, \varphi), \end{aligned}$$

which proves that

$$J^\epsilon(\overline{u^m}, \overline{u^c}, \overline{\varphi}) = \inf_{(u^m, u^c, \varphi) \in F_{ad}} J^\epsilon(u^m, u^c, \varphi).$$

Thus $(\overline{u^m}, \overline{u^c}, \overline{\varphi})$ is a minimizer of the problem (P^ϵ) . \square

Let $\varphi \in H^1(\Omega, \mathbb{R}) \cap L^\infty(\Omega, \mathbb{R})$. With help of the control-to-state operators $S^m(\varphi) = u^m$, $S^c(\varphi) = u^c$ the state functional $J^\epsilon(u^m, u^c, \varphi)$ can be viewed as being only dependent on the control φ , which defines the *reduced cost-functional* $j(\varphi)$

$$J^\epsilon(u^m, u^c, \varphi) = J^\epsilon(S^m(\varphi), S^c(\varphi), \varphi) =: j(\varphi).$$

Lemma 3.5. The reduced cost-functional $j : H^1(\Omega, \mathbb{R}) \cap L^\infty(\Omega, \mathbb{R}) \rightarrow \mathbb{R}$ is Fréchet-differentiable. The derivative in direction $\omega \in H^1(\Omega, \mathbb{R}) \cap L^\infty(\Omega, \mathbb{R})$ is

$$\begin{aligned} j'(\varphi)\omega &= -\langle \mathcal{E}(u^m), \mathcal{E}(u^m) \rangle_{C'(\varphi)\omega} + 2 \int_{\Omega} \omega g \cdot u^m \, dx \\ &\quad - \beta \sum_{h=1}^N \left[\langle \mathcal{E}(u_h^c), \mathcal{E}(u_h^c) \rangle_{C'(\varphi)\omega} - 2 \int_{\Omega_h} \omega g \cdot u_h^c \, dx \right] \\ &\quad + \gamma \epsilon \int_{\Omega} \nabla \varphi \cdot \nabla \omega \, dx + \frac{\gamma}{\epsilon} \int_{\Omega} \psi'(\varphi) \omega \, dx. \end{aligned}$$

Proof. The partial derivatives of J^ϵ are continuous by the sequence criterion. Using

$$\bar{u}^m = (S^m)'(\varphi)\omega$$

and

$$\bar{u}_h^c = (S_h^c)'(\varphi)\omega$$

leads to

$$\begin{aligned} j'(\varphi)\omega &= J_{u^m}^\epsilon(u^m, u^c, \varphi) (S^m)'(\varphi)\omega + \beta \sum_{h=1}^N J_{u_h^c}^\epsilon(u^m, u^c, \varphi) (S_h^c)'(\varphi)\omega + J_\varphi^\epsilon(u^m, u^c, \varphi)\omega \\ &= J_{u^m}^\epsilon(u^m, u^c, \varphi) \bar{u}^m + \beta \sum_{h=1}^N J_{u_h^c}^\epsilon(u^m, u^c, \varphi) \bar{u}_h^c + J_\varphi^\epsilon(u^m, u^c, \varphi)\omega \\ &= 2\langle \mathcal{E}(u^m), \mathcal{E}(\bar{u}^m) \rangle_{C(\varphi)} + 2\beta \sum_{h=1}^N \langle \mathcal{E}(u_h^c), \mathcal{E}(\bar{u}_h^c) \rangle_{C(\varphi)} \\ &\quad + \langle \mathcal{E}(u^m), \mathcal{E}(u^m) \rangle_{C'(\varphi)\omega} + \beta \sum_{h=1}^N \langle \mathcal{E}(u_h^c), \mathcal{E}(u_h^c) \rangle_{C'(\varphi)\omega} \\ &\quad + \gamma \epsilon \int_{\Omega} \nabla \varphi \cdot \nabla \omega \, dx + \frac{\gamma}{\epsilon} \int_{\Omega} \psi'(\varphi) \omega \, dx \\ &= -\langle \mathcal{E}(u^m), \mathcal{E}(u^m) \rangle_{C'(\varphi)\omega} + 2 \int_{\Omega} \omega g \cdot u^m \, dx \\ &\quad - \beta \sum_{h=1}^N \left[\langle \mathcal{E}(u_h^c), \mathcal{E}(u_h^c) \rangle_{C'(\varphi)\omega} - 2 \int_{\Omega_h} \omega g \cdot u_h^c \, dx \right] \\ &\quad + \gamma \epsilon \int_{\Omega} \nabla \varphi \cdot \nabla \omega \, dx + \frac{\gamma}{\epsilon} \int_{\Omega} \psi'(\varphi) \omega \, dx. \end{aligned} \tag{23}$$

Equation (18) was applied in the last equality. □

The special structure of the compliance causes the adjoint equations to coincide with the respective state equations. For adjoint states $q^m \in H_D^1(\Omega, \mathbb{R}^d)$ and $q_h \in H_D^1(\Omega_h, \mathbb{R}^d)$, $h = 1, \dots, N$

$$\begin{aligned} q^m &\equiv u^m, \\ q_h &\equiv u_h^c, \end{aligned} \quad h = 1, \dots, N$$

holds true.

The problem (P^ϵ) was defined using the functional $J^\epsilon(u^m, u^c, \varphi)$. After considering the reduced functional $j(\varphi)$ the optimality problem can be reformulated compactly as

$$\min_{\varphi \in \mathcal{G}^m} j(\varphi). \quad (24)$$

The following theorem summarizes preceding results.

Theorem 3.6. Let $\bar{\varphi} \in \mathcal{G}^m$ be a solution of (24). Since \mathcal{G}^m is convex the following optimality system holds

State Equations

$$\begin{aligned} \langle \mathcal{E}(v^m), \mathcal{E}(u^m) \rangle_{C(\varphi)} &= F(v^m, \varphi) & \forall v^m \in H_D^1(\Omega, \mathbb{R}^d), \\ \langle \mathcal{E}(v_h), \mathcal{E}(u_h^c) \rangle_{C(\varphi)} &= \int_{\Omega_h} \varphi g \cdot v_h \, dx & \forall v_h \in H_D^1(\Omega_h, \mathbb{R}^d), \quad h = 1, \dots, N \end{aligned}$$

Variational Inequality

$$\begin{aligned} &\gamma \int_{\Omega} \epsilon \nabla \varphi \cdot \nabla (\varphi - \bar{\varphi}) + \frac{1}{\epsilon} \psi'(\varphi) (\varphi - \bar{\varphi}) \, dx \\ &- \langle \mathcal{E}(u^m), \mathcal{E}(u^m) \rangle_{C'(\varphi)(\varphi - \bar{\varphi})} + 2 \int_{\Omega} (\varphi - \bar{\varphi}) g \cdot u^m \, dx \\ &- \beta \sum_{h=1}^N \left[\langle \mathcal{E}(u_h^c), \mathcal{E}(u_h^c) \rangle_{C'(\varphi)(\varphi - \bar{\varphi})} - 2 \int_{\Omega_h} (\varphi - \bar{\varphi}) g \cdot u_h^c \, dx \right] \\ &\geq 0 \quad \forall \varphi \in \mathcal{G}^m. \end{aligned}$$

Remark. Introduction of KKT multipliers for the control constraint

The optimality conditions can be derived formally via the *Lagrange functional*

$$\begin{aligned} \mathcal{L}(u^m, u^c, \varphi, v^m, v^c) &:= F(u^m, \varphi) + \beta P^d(u^c, \varphi) + \gamma E^\epsilon(\varphi) \\ &- \langle \mathcal{E}(u^m), \mathcal{E}(v^m) \rangle_{C(\varphi)} + F(v^m, \varphi) \\ &- \beta \sum_{h=1}^N \left[\langle \mathcal{E}(u_h^c), \mathcal{E}(v_h) \rangle_{C(\varphi)} - \int_{\Omega_h} \varphi g \cdot v_h \, dx \right]. \end{aligned}$$

When formulating the optimality system the box constraint $0 \leq \varphi \leq 1$ was taken into account via the space \mathcal{G}^m . In accordance with (Tröltzsch, 2010, p. 330–334) *Karush-Kuhn-Tucker multipliers* $\mu_+, \mu_- \in (L^\infty(\Omega))^*$ are introduced such that

$$\begin{aligned} 0 &\leq \varphi \leq 1 \quad \text{a.e. in } \Omega \\ \mu_+ &\geq 0, \mu_- \geq 0 \quad \text{in } \Omega \\ (\mu_+, \varphi - 1) &= 0, (\mu_-, -\varphi) = 0 \quad \text{in } \Omega. \end{aligned} \quad (25)$$

Here the notation

$$(p, q) = 0 \text{ in } \Omega \Leftrightarrow p(x) q(x) = 0 \quad \forall x \in \Omega$$

is used.

4 Discretization

Observations and theoretical derivations of linear elasticity take place in the three-dimensional space. However, two-dimensional models have computational advantages. At the beginning of this chapter a two-dimensional models will be studied. Then an interface propagation is explained, which allows stationary problems to be solved iteratively. Lastly the Primal-Dual Active-Set Method is presented to solve the optimal control problem.

The goal is to construct a thin, 3D-printable structure. The *plane stress* model is feasible since it assumes that the z -dimension is very small in comparison to the others.

The normal stress $\sigma_{z,z}$ and the shear stresses $\sigma_{x,z}$ and $\sigma_{y,z}$ are perpendicular to the x - y -plane. In the plane stress model they are assumed to be zero. Thus $\sigma_{i,z} = \sigma_{z,i} = 0$, $i = x, y, z$ and assuming symmetry leads to

$$\sigma = \begin{bmatrix} \sigma_{x,x} & \sigma_{x,y} & 0 \\ \sigma_{x,y} & \sigma_{y,y} & 0 \\ 0 & 0 & 0 \end{bmatrix}. \quad (26)$$

This yields $\mathcal{E}_{x,z} = 0$, $\mathcal{E}_{y,z} = 0$ and

$$\begin{aligned} 0 = \sigma_{z,z} &= \lambda \operatorname{tr}(\mathcal{E}) + 2\mu \mathcal{E}_{z,z} \Leftrightarrow (\lambda + 2\mu) \mathcal{E}_{z,z} = -\lambda (\mathcal{E}_{x,x} + \mathcal{E}_{y,y}) \\ &\Leftrightarrow \mathcal{E}_{z,z} = -\frac{\lambda}{\lambda + 2\mu} (\mathcal{E}_{x,x} + \mathcal{E}_{y,y}). \end{aligned}$$

Since the (z, z) -component of the strain tensor \mathcal{E} can be written as a linear combination of $\mathcal{E}_{x,x}$ and $\mathcal{E}_{y,y}$, the component $\mathcal{E}_{z,z}$ can be eliminated. However, the Lamé-constants have to be adapted to account for this. Hooke's material law reads

$$\begin{aligned} \sigma &= \lambda \operatorname{tr}(\mathcal{E}) I + 2\mu \mathcal{E} \\ &= \lambda (\mathcal{E}_{x,x} + \mathcal{E}_{y,y} + \mathcal{E}_{z,z}) I + 2\mu \mathcal{E} \\ &= \lambda \left(\mathcal{E}_{x,x} + \mathcal{E}_{y,y} - \frac{\lambda}{\lambda + 2\mu} (\mathcal{E}_{x,x} + \mathcal{E}_{y,y}) \right) I + 2\mu \mathcal{E} \\ &= \lambda \left(\frac{\lambda + 2\mu}{\lambda + 2\mu} (\mathcal{E}_{x,x} + \mathcal{E}_{y,y}) - \frac{\lambda}{\lambda + 2\mu} (\mathcal{E}_{x,x} + \mathcal{E}_{y,y}) \right) I + 2\mu \mathcal{E} \\ &= \lambda \left(\frac{2\mu}{\lambda + 2\mu} (\mathcal{E}_{x,x} + \mathcal{E}_{y,y}) \right) I + 2\mu \mathcal{E} \\ &= \underbrace{\frac{2\lambda\mu}{\lambda + 2\mu}}_{\lambda, \text{ adapted for the plane stress case}} (\mathcal{E}_{x,x} + \mathcal{E}_{y,y}) I + 2\mu \mathcal{E}. \end{aligned}$$

The goal is to iteratively solve the stationary problem. After an initial material distribution φ_0 is set, *pseudo timestepping* is used to evolve the solution. The negative derivative of the reduced cost functional is chosen as the direction of interface movement, thus

$$-j'(\varphi) \omega = -\frac{\partial \mathcal{L}}{\partial \varphi} \omega = \epsilon \int_{\Omega} \frac{\partial \varphi}{\partial t} \omega \, dx \approx \epsilon \int_{\Omega} \frac{\varphi^{k+1} - \varphi^k}{\tau} \omega \, dx, \quad (27)$$

where τ is the length of a pseudo time-step. This approach was developed in the work of (Cahn &

Hilliard, 1958) and (Allen & Cahn, 1979). Inserting the derivative (23) leads to

$$\begin{aligned} \epsilon \int_{\Omega} \frac{\partial \varphi}{\partial t} \omega \, dx &= -\gamma \epsilon \int_{\Omega} \nabla \varphi \cdot \nabla \omega \, dx - \frac{\gamma}{\epsilon} \int_{\Omega} \psi'(\varphi) \omega \, dx \\ &\quad + \langle \mathcal{E}(u^m), \mathcal{E}(u^m) \rangle_{C'(\varphi)\omega} \, dx - 2 \int_{\Omega} \omega \mathbf{g} \cdot u^m \, dx \\ &\quad + \beta \sum_{h=1}^N \left[\langle \mathcal{E}(u_h^c), \mathcal{E}(u_h^c) \rangle_{C'(\varphi)\omega} - 2 \int_{\Omega_h} \omega \mathbf{g} \cdot u_h^c \, dx \right]. \end{aligned} \quad (28)$$

Towards better stability the equation is discretized using a semi-implicit approach and approximation (27) is applied

$$\begin{aligned} &\frac{\epsilon}{\tau} \int_{\Omega} \varphi^{k+1} \omega \, dx + \gamma \epsilon \int_{\Omega} \nabla \varphi^{k+1} \cdot \nabla \omega \, dx \\ &\approx \frac{\epsilon}{\tau} \int_{\Omega} \varphi^k \omega \, dx - \frac{\gamma}{\epsilon} \int_{\Omega} \psi'(\varphi^k) \omega \, dx \\ &\quad + \langle \mathcal{E}(u^m), \mathcal{E}(u^m) \rangle_{C'(\varphi^k)\omega} \, dx - 2 \int_{\Omega} \omega \mathbf{g} \cdot u^m \, dx \\ &\quad + \beta \sum_{h=1}^N \left[\langle \mathcal{E}(u_h^c), \mathcal{E}(u_h^c) \rangle_{C'(\varphi^k)\omega} - 2 \int_{\Omega_h} \omega \mathbf{g} \cdot u_h^c \, dx \right]. \end{aligned} \quad (29)$$

Note that the time-step τ is just a numerical construct and does not represent a physically relevant time, hence the word pseudo. The time-step can be varied independently of any physical phenomenon to achieve convergence.

The box constraint for the phase field is made up of the two inequalities $-\varphi(x) \leq 0$ and $\varphi(x) - 1 \leq 0$. For example the second inequality is called *active* in $x \in \Omega$ if $\varphi(x) - 1 = 0$ and *inactive* if $\varphi(x) - 1 < 0$. Adding the equations of (25) to the Lagrange function yields

$$\mathcal{L} := \mathcal{L} - (\mu_+, \varphi - 1) - (\mu_-, -\varphi),$$

leading to the unconstrained optimality problem

$$\min_{\varphi \in H^1(\Omega, \mathbb{R})} \mathcal{L}.$$

In an optimum

$$\frac{\partial \mathcal{L}}{\partial \varphi} \omega = \frac{\partial \mathcal{L}}{\partial \varphi} \omega - \mu_+ \omega + \mu_- \omega \stackrel{!}{=} 0 \quad (30)$$

holds.

This incorporation of the box constraint via KKT-multipliers leads to the *Primal-Dual Active-Set Method*, see (Blank *et al.*, 2013). In each step the active and inactive sets are updated using the result from the previous iteration. If there are no further changes in these sets, the algorithm has converged and terminates.

Algorithm 1 Primal-Dual Active-Set-Method

1: Initialize

$$\varphi^0, \mu_+^0, \mu_-^0 \text{ and set } k = 0.$$

2: Solve the mechanical system (6), yielding u^m .Solve the AMC systems (14), $h = 1, \dots, N$ yielding u_h^c , $h = 1, \dots, N$.3: With $c \in \mathbb{R}_+$ set

$$\begin{aligned} \mathcal{A}_+^{k+1} &:= \{x \in \Omega : \mu_+^k(x) + c(\varphi^k(x) - 1) > 0\}, \\ \mathcal{A}_-^{k+1} &:= \{x \in \Omega : \mu_-^k(x) + c(-\varphi^k(x)) > 0\}, \\ \mathcal{I}^{k+1} &:= \Omega \setminus (\mathcal{A}_+^{k+1} \cup \mathcal{A}_-^{k+1}) \end{aligned}$$

and

$$\begin{aligned} \varphi^{k+1} &= 1 \text{ on } \mathcal{A}_+^{k+1}, \\ \varphi^{k+1} &= 0 \text{ on } \mathcal{A}_-^{k+1}, \\ \mu_+^{k+1} &= 0 \text{ on } \Omega \setminus \mathcal{A}_+^{k+1}, \\ \mu_-^{k+1} &= 0 \text{ on } \Omega \setminus \mathcal{A}_-^{k+1}. \end{aligned}$$

4: On \mathcal{I}^{k+1} solve

$$\begin{aligned} & \frac{\epsilon}{\tau} \int_{\Omega} \varphi^{k+1} \omega \, dx + \gamma \epsilon \int_{\Omega} \nabla \varphi^{k+1} \cdot \nabla \omega \, dx \\ &= \frac{\epsilon}{\tau} \int_{\Omega} \varphi^k \omega \, dx - \frac{\gamma}{\epsilon} \int_{\Omega} \psi'(\varphi^k) \omega \, dx \\ &+ \langle \mathcal{E}(u^m), \mathcal{E}(u^m) \rangle_{C'(\varphi^k)\omega} \, dx - 2 \int_{\Omega} \omega g \cdot u^m \, dx \\ &+ \beta \sum_{h=1}^N \left[\langle \mathcal{E}(u_h^c), \mathcal{E}(u_h^c) \rangle_{C'(\varphi^k)\omega} - 2 \int_{\Omega_h} \omega g \cdot u_h^c \, dx \right]. \end{aligned} \tag{31}$$

for φ^{k+1} .5: On \mathcal{A}_+^{k+1} calculate μ_+^{k+1} via (30).6: On \mathcal{A}_-^{k+1} calculate μ_-^{k+1} via (30).7: **Stop** or set $k = k + 1$ and return to 2.

The potential ψ introduced in Section 2.3 has a local maximum in $\varphi = 0.5$. As an initialization a slight perturbation around 0.5 is empirically beneficial. According to empirical evidence $c = 100$ is a good choice. The elasticity equations and the gradient equation are solved via the *Finite Element Method*. According to the work of (Hintermüller *et al.*, 2002) the Primal-Dual Active-Set-Method can be interpreted as a semismooth Newton method. This yields local superlinear convergence.

5 Numerical Examples

Calculations are done for a simply supported beam with and without the Additive Manufacturing Constraint. This makes it possible to observe the influence of the constraint. Here only linearly elastic, homogeneous, isotropic materials are considered. For a formal definition see (Braess, 2013). The elastic moduli depend on the type of material. Since the aim is to model 3D-printable structures, the properties of typical filament, PLA, will be used. The code is implemented in C/C++ and incorporates the `pDelib` toolbox for numerical computations, see (Streckenbach *et al.*, 2014).

5.1 Calculations without Additive Manufacturing Constraint

Three parameters can be varied to influence the topologies resulting from the Primal-Dual Active-Set-Method. It will be seen why the parameter γ characterizes the surface tension and the value of ϵ determines the interface width. The volume constraint parameter m determines how much material is used. The first part of the cost function, the compliance, is the inverse of the structural stiffness.

These calculations are performed without taking the Additive Manufacturing Constraint into account. This is achieved by setting $\beta = 0$. In this subsection the cost functional is defined via

$$\underbrace{J^\epsilon(u^m, \varphi)}_{\text{Residuum}} := \underbrace{F(u^m, \varphi)}_{\text{Compliance}} + \gamma E^\epsilon(\varphi).$$

5.1.1 Parameter Study for ϵ and γ

In this study the following nondimensionalized parameters will be used:

Force density	$f = -6000$
Interface width parameter	$\epsilon_0 = 0.0035$
Surface tension parameter	$\gamma_0 = 2.5 \times 10^{-5}$
Volume constraint	$m = 20\%$

Table 1: Top: Compliance Value. Bottom: Residuum Value

$\epsilon \backslash \gamma$	$\frac{1}{64}\gamma_0$	$\frac{1}{32}\gamma_0$	$\frac{1}{16}\gamma_0$	$\frac{1}{8}\gamma_0$	$\frac{1}{4}\gamma_0$	$\frac{1}{2}\gamma_0$	γ_0
$\frac{1}{2}\epsilon_0$				0.001442 0.001477			
ϵ_0	0.001519 0.001535	0.001467 0.001488	0.001430 0.001463	0.001400 0.001454	0.001408 0.001487	0.001445 0.0015496	0.001478 0.00163
$2\epsilon_0$				0.001404 0.001485			
$4\epsilon_0$				0.001414 0.001521			

The parameter γ is the prefactor of the Ginzburg-Landau term and thus controls the influence of the perimeter regularization, which can be interpreted as a surface tension. Larger values of γ cause the material to lump together to simple, non-filigree structures. A sensibly small γ allows for the creation of more filigree structures while still avoiding checkerboarding. As a reminder, the Ginzburg-Landau penalty term is defined via

$$E^\epsilon(\varphi) = \int_{\Omega} \frac{\epsilon}{2} |\nabla \varphi|^2 + \frac{1}{\epsilon} \psi(\varphi) \, dx. \quad (32)$$

The parameter ϵ regulates the influence of the two summands within the Ginzburg-Landau term. When ϵ is increased the gradient term receives a higher weight. Penalizing the derivative causes less jumps to occur. However, impure phases with $0 < \varphi < 1$ are more likely to appear. Often ϵ is referred to as the interface thickness parameter. If it is set too large filigree structures cannot emerge. When ϵ is decreased a transition from material to void is penalized less. A smaller interface thickness brings about more filigree structures. If ϵ is very small the potential term dominates. Fine, pure phased, porous structures arise. It helps to decrease the mesh size, which allows for thinner beams to be displayed. These influences of the parameters ϵ and γ are summarized in Figure 1.

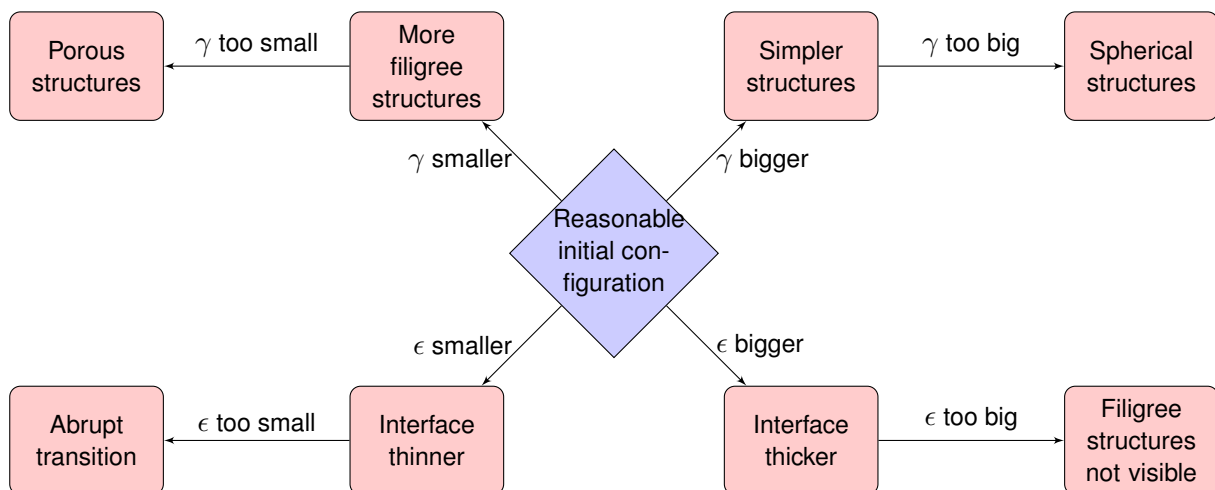


Figure 1: Influence of parameters

5.2 Calculations with Additive Manufacturing Constraint

The numerical results discussed in Section 5.1 did not take the Additive Manufacturing Constraint into consideration. After having seen how the parameters γ and ϵ influence the compliance, it is time to introduce the AMC. Its purpose is to ensure that a 3D printer will be able to print the resulting topology. The penalty term was introduced in Chapter 2.4. The sum of intermediate compliances is added to the cost functional to increase stiffness during the building process. One would assume that the penalty term causes overhangs to vanish or supporting structures to arise, which will decrease deformations during the printing process.

In order to test the influence of AMC, calculations are done for different factors β . From an analytical point it is not trivial to see how severely the penalty term influences the optimal topology. A set of calculations is performed to gather intelligence numerically.

For every layer an elasticity equation is solved. More layers model the building process more precisely, but increase the computation cost significantly. The constraint problems can be solved independent from one another. If a larger number of layers is required, parallelization is a feasible option. Here the number of layers is set to just three. The computational cost is kept small and influences can already be seen.

In Table 1 it has been found that a configuration with $\epsilon = \epsilon_0$ and $\gamma = \frac{1}{8}\gamma_0$ leads to a minimal compliance and thus maximal stiffness. A volume constraint of $m = 20\%$ results in reasonable filigree and at the same time stiff structures. These parameters are kept constant while examining the influence of the penalty function.

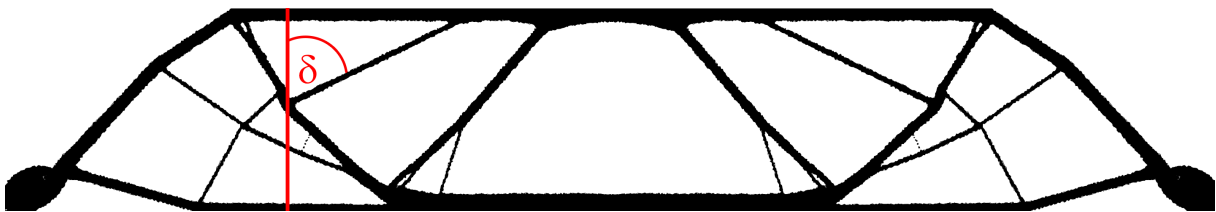


Figure 2: Structure without AMC, $\beta = 0$

Figure 2 depicts the structure without influence of the AMC, i.e. $\beta = 0$. Large holes show that the material is not scattered, but concentrated in major beams. Not a lot of support structures are present to hold the major beams in place. Generally the severity of an overhang can be measured by its angle to the normal axis. As a rule of thumb, an angle of over 45° is critical. Here diagonal structures can be seen that have an angle δ to the vertical axis of well above 45° . Also note how the material is distributed evenly with respect to the vertical axis. It is not the case that a majority of the material is placed either near the top or the bottom of the domain.

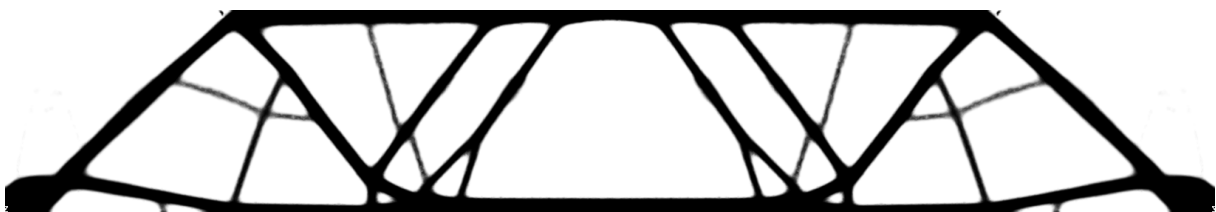
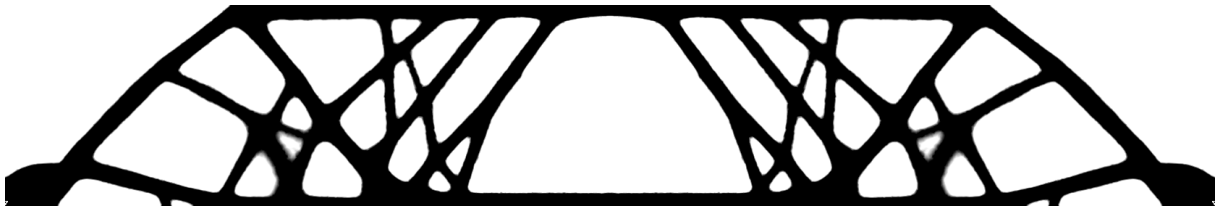


Figure 3: Structure with AMC, $\beta = 64$

The penalty term is introduced by successively doubling the factor β . A convincing change in topology can be seen when β reaches 64, see Figure 3. The beams are quite vertical, i.e. have a small angle towards the normal vector and thus can be printed. These beams do not have a big impact on the compliance. In other areas of the domain more substructures have emerged. These mostly vertical supports lower the compliance in intermediate domains. In the technical realm they allow for less deformations in the manufacturing process.

Figure 4: More support structures, $\beta = 128$

Doubling the factor β once more leads to an increase in support structures displayed in Figure 4. A larger amount of material is placed near the bottom of the domain as opposed to the vertically even distribution found in Figure 2. This leads to a lower compliance in the advanced stages of manufacturing. Beams are oriented more vertically than before. In Figure 2 the beams were quite long, whereas here they intersect each other. The leverage effect causes a smaller amount of deformation and stress on these shorter beams, which makes the structure more stable.

Note that it looks like more material was used in the last computation. This is not the case. However, an increase of β leads to a larger influence of compliances in the cost functional. This is similar to choosing a smaller γ , which would mean less influence of the Ginzburg-Landau term. Thus impure phases are not penalized as much, which results in larger interfaces. A cutoff at the value 0.5 makes these structures appear to be using more material.

Figure 5: AMC term too large, $\beta = 512$

If β is too large, the AMC penalty term dominates the cost functional, which can be seen in Figure 5. Towards lowering intermediate compliances, material is placed almost exclusively near the bottom of the domain. This causes the structure to be extremely stable during the manufacturing process. On the other hand, there is very little material used to bear the weight of a load. The resulting deformations are large as is the compliance. However, this effect is largely ignored because of the dominating penalty term. This defeats the purpose of building a bridge which is ultimately meant to withstand exterior forces.

Up to this point the influence of the Additive Manufacturing Constraint was isolated by only varying the parameter β . The study conducted in Section 5.1.1 shows how γ and ϵ affect the topology. Insights from isolating all three parameters allow for a fine-tuning of support structures. As an example some topologies are displayed. The first two arise from setting $\beta = 64$ and varying the interface thickness by adjusting ϵ .

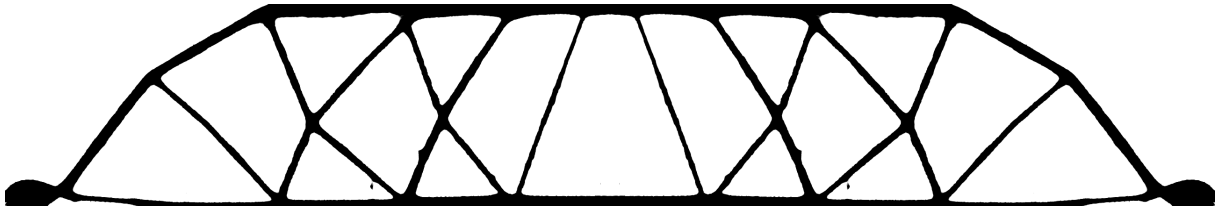


Figure 6: $\epsilon = 4\epsilon_0$, $\gamma = \frac{1}{8}\gamma_0$, $\beta = 64$

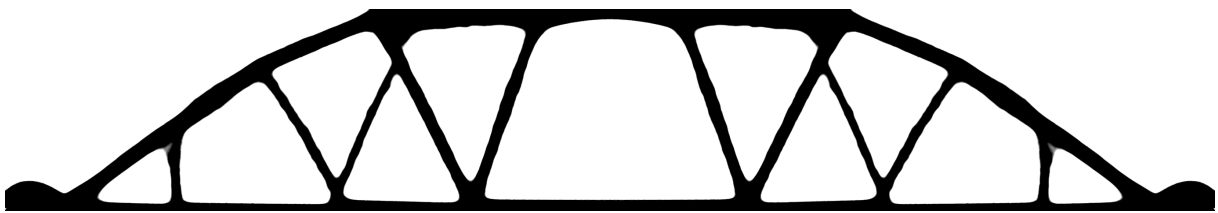


Figure 7: $\epsilon = 8\epsilon_0$, $\gamma = \frac{1}{8}\gamma_0$, $\beta = 64$

The parameter β is doubled and thereby the influence of the AMC increased. When the calculations are repeated more support structures appear to stabilize the topology during Additive Manufacturing.

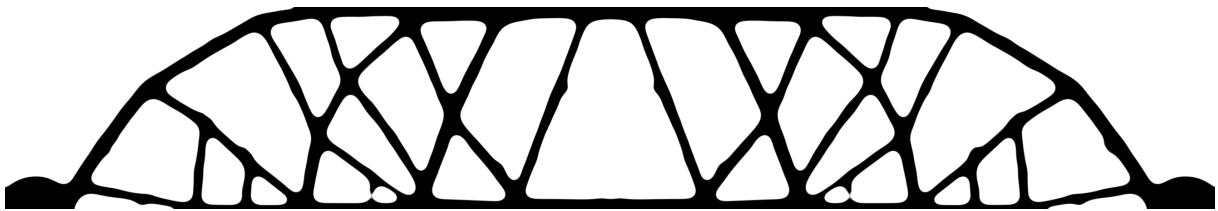


Figure 8: $\epsilon = 4\epsilon_0$, $\gamma = \frac{1}{8}\gamma_0$, $\beta = 128$

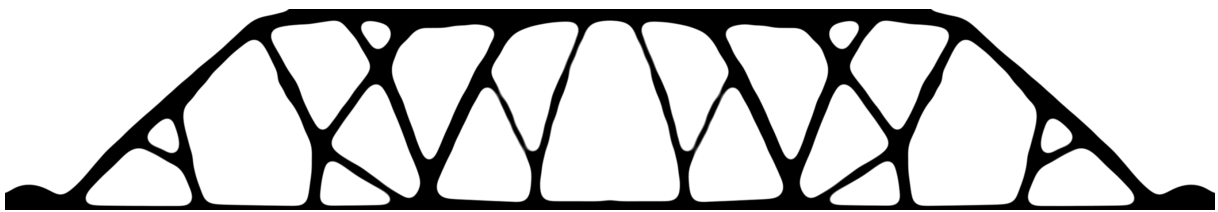


Figure 9: $\epsilon = 8\epsilon_0$, $\gamma = \frac{1}{8}\gamma_0$, $\beta = 128$

5.3 Multiple Loads

As a second example a multi load case is considered. To goal is to design a 3D printable wheel. To ensure placement of material on the border the phase field φ is set to 1 for points in the outmost 5% of the domain.

The building domain for the load case is seen in Figure 10a. Loads with direction towards the midpoint of the left side of the domain are acting upon all points of the green boundary. A Dirichlet boundary is defined via the blue edge of the inner semicircle. The red vertical lines indicate a symmetry axis.

When considering the elasticity problems stemming from the Additive Manufacturing Constraint only gravity is acting upon the structure. Here the boundary conditions are different, which is depicted in Figure 10b. The domain is fixed on a printer bed, which is modeled via a Dirichlet boundary along the blue line. A homogeneous Neumann condition is defined on the red border. See .

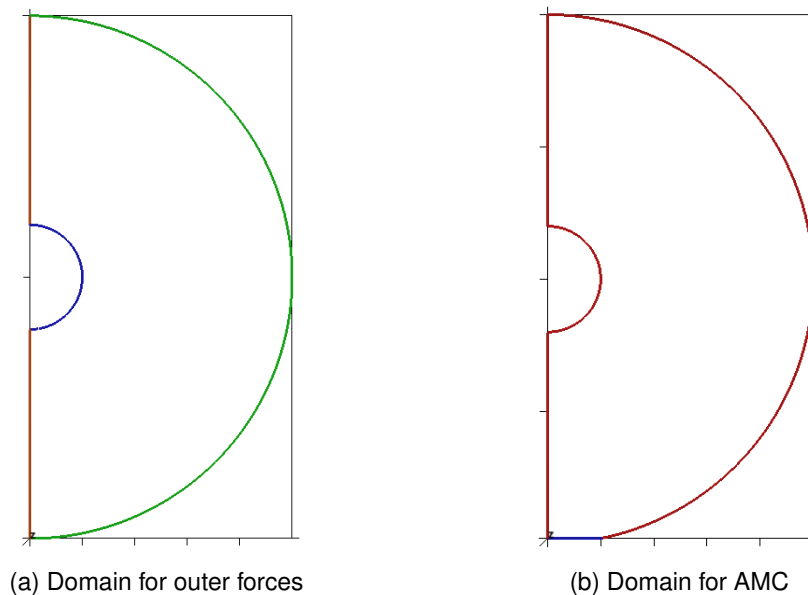


Figure 10: Boundary conditions for the load case and the manufacturing case

Again the influence of the Additive Manufacturing Constraint is investigated. Figure 11a shows the result if the AMC is inactive. Large horizontal structures arise and the material distribution is almost symmetrical with regards to the horizontal axis. The introduction of the AMC in Figure 11b leads to thinner overhangs, decreasing compliances of gravity-based elasticity problems. Instead this material is placed towards the horizontal center. The increasing trend of ticker structures near the bottom of the domain is continued in Figure 11c. The trade-off between supporting mechanical outer forces and stability during the printing process is observed anew. If the prefactor β is chosen too large the material contracts like a pillar on top of the Dirichlet boundary, see Figure 11d. This does decrease printing instabilities, but the structure would not support external loads well.

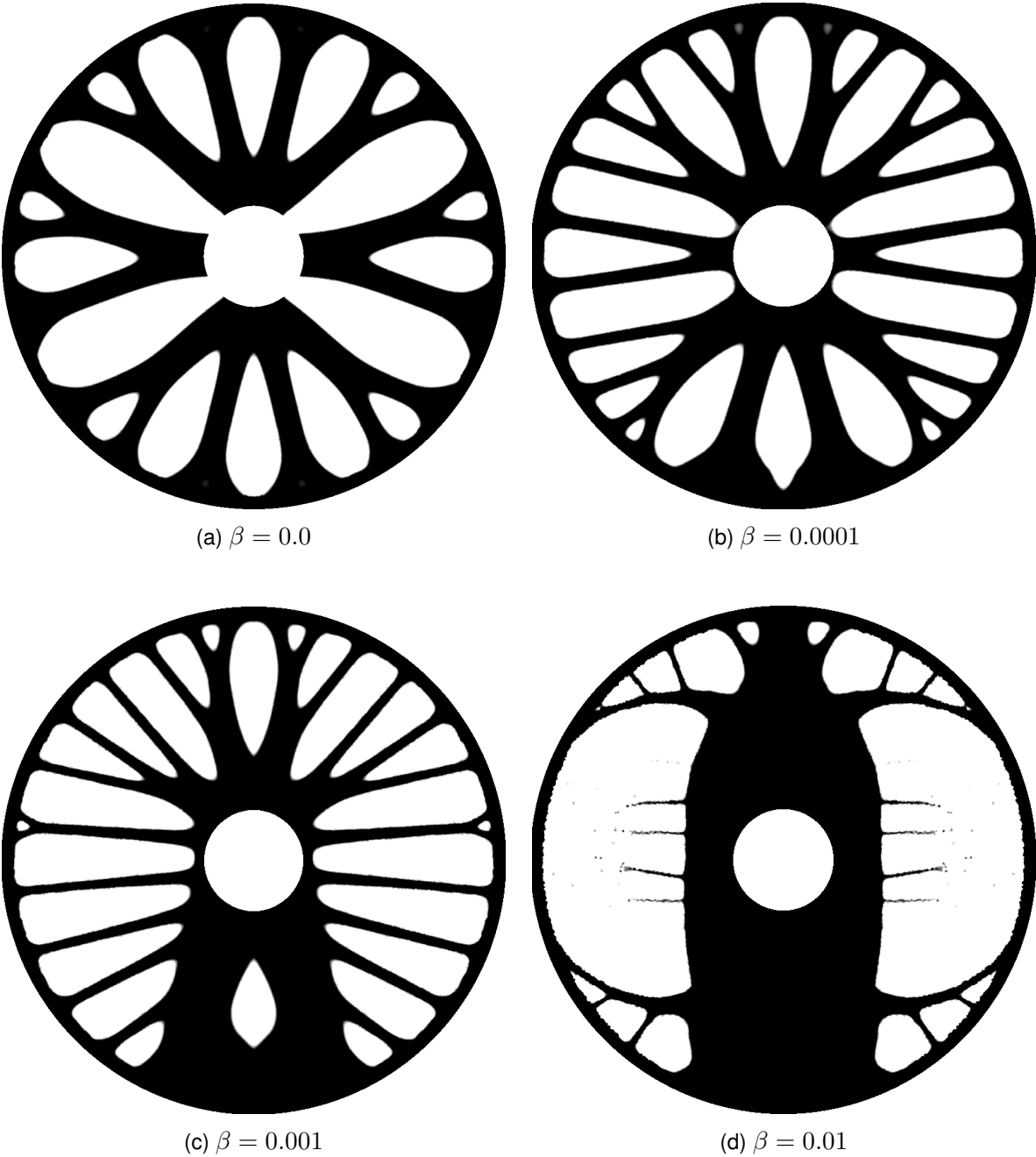


Figure 11: Influence of the Additive Manufacturing Constraint

6 Conclusion

This paper comprises five conceptual levels. First, instabilities during 3D Printing motivate research on this topic. Secondly, the Additive Manufacturing Constraint gets incorporated into the optimal control problem. Optimality conditions arise from a rigorous analysis. The fourth level builds upon those results when discussing the numerical approach. Lastly, calculations show that the Additive Manufacturing Constraint decreases overhangs and brings about support structures, which validates this concepts.

The approach of modeling material distribution via a phase field stems from (Blank *et al.* , 2012) with an analysis found in (Blank *et al.* , 2014). A penalty function for the Additive Manufacturing Constraint is introduced by (Allaire *et al.* , 2017a).

To the author's best knowledge this is the first time the AMC is applied to the phase field method for Topology Optimization. A rigorous analysis of the optimal control problem shows existence of a solution and results in first order necessary optimality conditions.

An Allen-Cahn interface propagation iteratively solves the stationary optimality problem. After a pseudo time discretization the Primal Dual Active Set Algorithm is executed. Calculations without the AMC show in which way the topology can be influenced by setting the parameters. After applying the AMC noticeable changes occur. More support structures emerge, leading to a smaller compliance and in turn to a higher stiffness during the manufacturing process. The influence of the penalty term is adjustable, which allows the structures to be fine-tuned according to engineering demands. No labor intensive post processing is necessary, giving this approach a big advantage over manually added support structures. Applying the AMC to the phase field method was successful.

Further research on this topic could include the incorporation of a micro field to represent lattice structures. This helps create printable light-weight constructions. Additionally, one could implement an adaptive mesh, which is fine in the interface region and coarser otherwise. This would reduce computational costs and allow for three dimensional calculations. An integration of stress constraints is desirable for engineering applications. On a larger scope there are many more problems in Additive Manufacturing which can be tackled with optimization methods.

References

- Allaire, Grégoire, Jouve, François, & Toader, Anca-Maria. 2004. Structural optimization using sensitivity analysis and a level-set method. *Journal of Computational Physics*, **194**(1), 363–393.
- Allaire, Grégoire, Dapogny, Charles, Faure, Alexis, & Michailidis, Georgios. 2017a. Shape optimization of a layer by layer mechanical constraint for additive manufacturing. *Comptes Rendus Mathématique*, **355**(6), 699–717.
- Allaire, Grégoire, Dapogny, Charles, Estevez, Rafael, Alexis, Faure, & Michailidis, Georgios. 2017b. Structural optimization under overhang constraints imposed by additive manufacturing technologies. *Journal of Computational Physics*, **351**, 295–328.
- Allen, Samuel, & Cahn, John. 1979. A microscopic theory for antiphase boundary motion and its application to antiphase domain coarsening. *Acta Metallurgica*, **27**(6), 1085–1095.
- Ambrosio, Luigi, & Buttazzo, Giuseppe. 1993. An Optimal Design Problem with Perimeter Penalization. *Calculus of Variations*.

- Blank, Luise, Garcke, Harald, Sarbu, Lavinia, Srisupattarawanit, Tarin, Styles, Vanessa, & Voigt, Axel. 2012. Phase-field approaches to structural topology optimization. *Pages 245–256 of: Constrained Optimization and Optimal Control for Partial Differential Equations*. Springer.
- Blank, Luise, Garcke, Harald, Sarbu, Lavinia, & Styles, Vanessa. 2013. Primal-dual active set methods for Allen–Cahn variational inequalities with nonlocal constraints. *Numerical Methods for Partial Differential Equations*, **29**(3), 999–1030.
- Blank, Luise, Garcke, Harald, Farshbaf-Shaker, M Hassan, & Styles, Vanessa. 2014. Relating phase field and sharp interface approaches to structural topology optimization. *ESAIM: Control, Optimisation and Calculus of Variations*, **20**(4), 1025–1058.
- Bourdin, Blaise; Chambolle, Antonin. 2003. Design-dependent loads in topology optimization. *ESAIM: Control, Optimisation and Calculus of Variations, Volume 9 (2003)*, 19–48.
- Braess, Dietrich. 2013. *Finite Elemente in der Mechanik elastischer Körper*. Berlin, Heidelberg: Springer Berlin Heidelberg. 275–352.
- Cahn, John, & Hilliard, John. 1958. Free energy of a nonuniform system. I. Interfacial free energy. *The Journal of Chemical Physics*, **28**(2), 258–267.
- Eigel, Martin, Neumann, Johannes, Schneider, Reinhold, & Wolf, Sebastian. 2018. Risk averse stochastic structural topology optimization. *Computer Methods in Applied Mechanics and Engineering*, **334**, 470–482.
- Ginzburg, Vitaly, & Landau, Lev. 1950. On the Theory of superconductivity (In Russian). 20, 1064. English translation in: L. D. Landau, *Collected papers* (Oxford: Pergamon Press, 1965), 546.
- Hintermüller, Michael, Ito, Kazufumi, & Kunisch, Karl. 2002. The primal-dual active set strategy as a semismooth Newton method. *SIAM Journal on Optimization*, **13**(3), 865–888.
- Scalapino, Douglas, Sears, M, & Ferrell, Richard. 1972. Statistical mechanics of one-dimensional Ginzburg-Landau fields. *Physical Review B*, **6**(9), 3409.
- Shukla, Avinash, Misra, Anadi, & Kumar, Sunil. 2013. Checkerboard problem in finite element based topology optimization. *International Journal of Advances in Engineering & Technology*, **6**(4), 1769.
- Streckenbach, Timo, Fuhrmann, Jürgen, Langmach, Hartmut, & Uhle, Manfred. 2014. Pdelib - a software toolbox for numerical computations. URL: <http://www.pdelib.org>.
- Takezawa, Akihiro, Nishiwaki, Shinji, & Kitamura, Mitsuru. 2010. Shape and topology optimization based on the phase field method and sensitivity analysis. *Journal of Computational Physics*, **229**(7), 2697–2718.
- Tröltzsch, Fredi. 2010. *Optimal Control of Parial Differential Equations, Theory Methods and Applications*. American Mathematical Society.
- Van Gennip, Yves, Bertozzi, Andrea, *et al.* . 2012. Gamma-convergence of graph Ginzburg-Landau functionals. *Advances in Differential Equations*, **17**(11/12), 1115–1180.